Research Article

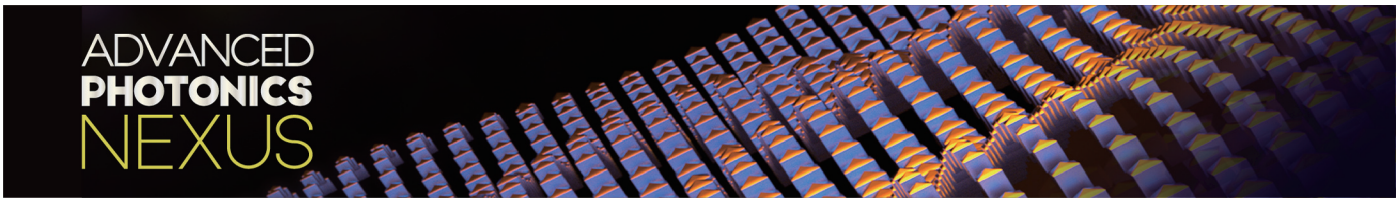

Angle-robust plasmonic color printing of deep subwavelength nanopixelated sodium metasurfaces

Jie Liang,[a,†] Yurui Qu,[b,†] Huizhen Zhang,[a] Yuhan Yang,[a] Yang Wang,[c] Yuchen Zhang,[a] Zhenda Lu,[a] Shining Zhu,[a] and Lin Zhou[a,*]

[a]Nanjing University, College of Engineering and Applied Sciences, National Laboratory of Solid State Microstructures, Key Laboratory of Intelligent Optical Sensing and Manipulation, Nanjing, China

[b]ShanghaiTech University, School of Information Science and Technology, Shanghai, China

[c]Beijing Institute of Technology, School of Physics, Key Lab of Advanced Optoelectronic Quantum Architecture and Measurement (Ministry of Education), Beijing Key Lab of Nanophotonics & Ultrafine Optoelectronic Systems, Beijing, China

Abstract. Plasmonic colors are attracting attention for their subwavelength small size, vibrant hues, and environmental sustainability beyond traditional pigments while suffering from angular and/or polarization dependency due to distinct excitations of lattice resonances and/or surface plasmon polaritons (SPPs). Here, we demonstrate the sodium metasurface-based plasmonic color palettes with polarization-independent wide-view angle (approximately $>\pm 60$ deg in experiment and up to ± 90 deg in theory) and single-particle-level pixel size (down to ~ 60 nm) that integrate both pigment-like and structure coloring advantages, fabricated by the templated nanorod-pixelated solidification of wetted liquid metals. Such intriguing performances are mainly attributed to the particle plasmon dominant spectral response by steering the filling profile and thus the interplay between localized surface plasmons and SPPs. Combining low material cost, potentially scalable manufacturing process, and pronounced optical performance, the proposed sodium-based metasurfaces will provide a promising route for advanced color information technology.

Keywords: angle-robust plasmonic color; sodium metal; deep subwavelength nanopixel; localized surface plasmon resonance; color printing.

Received Sep. 24, 2024; revised manuscript received Nov. 10, 2024; accepted for publication Dec. 3, 2024; published online Jan. 6, 2025.

[DOI: 10.1117/1.APN.4.1.016006]

1 Introduction

Structural color, generated by interference, diffraction, and/or scattering of light through versatile natural or artificial microstructures, has attracted tremendous interest for centuries[1] because of on-demand applications, including sensors, displays, and colorful solar cells.[2–4] A range of artificial structures employing spectral or diffusive reflection—such as photonic crystals, metamaterials, and pseudo-bandgap structures—has been developed, achieving remarkable advantages in coloration efficiency, durability, and tunability that extend beyond conventional pigmentation methods.[5–11] Among these, all-dielectric materials with high refractive indices and minimal visible region losses offer a promising approach to structural colors, though often constrained by limited spatial resolution.[7,12,13] In contrast, plasmonic nanostructures address this limitation by enabling nanoscale pixelation, which improves spatial resolution and enhances color information capacity, offering clear benefits for applications such as subwavelength photoprinting, integration, and miniaturization of color displays and imaging systems.[2,14,15] However, most periodic structural plasmonic colors [favorable for scalable and complementary metal oxide semiconductor (CMOS)-compatible fabrication] suffer from strong angular dispersion due to undiffractive surface waves, surface plasmon polaritons (SPPs), and other related lattice effects.[2,16,17] This

*Address all correspondence to Lin Zhou, linzhou@nju.edu.cn

†These authors contributed equally to this work.

inherent trade-off between pixel size reduction and angular stability, driven by strong interparticle coupling, makes conventional visible-range plasmonic nanostructures less competitive than pigments for achieving wide-view angle coloration.[2,18,19]

To address the issue of strong angular dispersion in plasmonic color, more refined plasmonic structures—such as deeply perforated metallic gratings, metal–dielectric–metal geometries with optically thick films, and random nanostructures—have been proposed to enhance angular tolerance.[20–30] However, the complexity, high cost, and often low optical contrast of these designs have limited the practical applications of plasmonic coloring nanostructures.

Nonnoble-metal plasmonic alternatives, such as sodium, have recently emerged as highly promising materials for low-loss plasmonic devices operating in both visible and near-infrared regions.[31–40] However, as with most plasmonic metasurface-based structural colorations, nearly all existing devices exhibit angle- and polarization-dependent optical spectra due to periodic nanostructures that activate SPP modes. In this work, we present a periodic plasmonic color palette based on sodium nanorods, achieved through the strategic optical design of nanorod micro-pixels and controlled templated solidification of liquid sodium. This design experimentally achieves angle tolerance up to ± 60 deg (limited by the objective lens of the measurement system) and pixel sizes as small as ~ 60 nm using simple periodic metasurfaces. Our results provide a new pathway toward sustainable, angle-robust, pigment-like colors with high scalability, and plasmon-enhanced spatial resolution.

2 Materials and Methods

2.1 Fabrication of Sodium Nanorod Arrays

A templated solidification process of liquid metals (TSLM) was carefully designed to fabricate sodium nanorod arrays. Initially, a 30-nm Ag film was deposited onto a 0.5-mm-thick quartz substrate via physical vapor deposition (Gatan 682). Periodic nanoholes were then patterned on the quartz substrate using focused ion beam (FIB) milling (dual-beam FIB 235, FEI Strata). Throughout the fabrication, the morphology and structural evolution were analyzed with scanning electron microscopy (SEM, dual-beam FIB 235, FEI Strata). After FIB processing, the Ag film on the quartz surface was removed with HNO_3. Next, the TSLM process was carried out to create the Na nanorod metasurface using a thermo-assisted spin-coating method on the nanohole-patterned quartz substrate. To remove the oxide shell, the sodium droplet was heated to ~ 120°C in an inert atmosphere glove box and then gently peeled using tweezers. The pretreated sodium droplet was then applied to the center of the spinning quartz (6000 rpm), forming the sodium nanorod arrays. Finally, once encapsulated in epoxy, the sodium nanostructures could be transferred out of the glove box without reactivity concerns.

2.2 Optical Measurements

The measurement of the reflection spectra and the optical microscope micrographs as a function of the incident angle was carried out through an angle-resolved micro-spectroscopy system (ARM available from ideaoptics, Shanghai, China) with $\times 100$ objective (0.9 NA and maximal angle 63 deg). Other common optical images were acquired with an optical microscope (Nikon, LV100ND) with $\times 10$ (0.3 NA) and $\times 20$ (0.45 NA) air objectives at Kohler illumination, using a DS-Fi2 Microscope Camera (CCD). The dark-field optical image and scattering spectra were measured by the microscope (Axio Imager.A2m, Zeiss, Oberkochen, Germany), with an objective lens ($\times 50$/0.8 NA, EC Epiplan-NEOFLUAR, Zeiss). The scattering spectrum was recorded by a grating spectrometer (Kymera 193i-A, Andor) and a CCD (iKon-M, Andor).

2.3 Numerical Simulation

The finite-difference time-domain (FDTD) simulation was conducted to calculate the electromagnetic fields and angle-resolved reflection spectra of the array (Lumerical FDTD Solutions, V8.6). In the simulation, we employed a unit cell with periodic boundary conditions and Bloch/periodic plane wave types under normal incidence, and infinite periodic Bloch boundary conditions are applied in $x - y$ dimensions with broadband fixed angle source technique (BFAST) plane wave type under oblique incidence to simulate periodic nanostructures. Perfectly matched layer boundary conditions are utilized in the vertical direction to prevent multiple reflections. The complex refractive indices of sodium metal and silver are from the previous research work[33] and Palik data, respectively. The refractive index of the SiO_2 spacing layer and substrate is set to 1.46.

3 Results and Discussion

The proposed plasmonic color palette based on Na nanorods features subwavelength pixels organized according to the cyan, magenta, and yellow subtractive color system, as schematically illustrated in Fig. 1(a). An ideal angle- and period-robust plasmonic structure should exhibit particle plasmon [or localized surface plasmon (LSP)]-dominated spectral responses while minimizing lattice-related surface resonances and SPP effects. Na nanorod-based metasurfaces represent ideal candidates due to two unique advantages stemming from both structural and material properties. (1) The excitation efficiency of lattice-related optical modes is highly influenced by the nanopixel filling profile. As shown in the calculated reflectance spectra in Fig. 1(b), sodium metasurfaces demonstrate significantly weaker SPP effects compared with their noble metal counterparts, with the Na nanorod-based metasurface exhibiting virtually no observable SPP signature. The period-dependent reflectance spectra (Fig. S2 in the Supplementary Material) further illustrate that the absorption dip of the Na nanorod metasurface remains largely insensitive to the unit cell period (p), resulting in a broader full width at half maximum (FWHM). This behavior can be attributed to the suppression of SPP effects and the dominance of the localized surface plasmon resonance (LSPR) mode, featuring strong field confinement and weak coupling effects. In contrast, the optical modes of Na films and Na nanohole metasurfaces are significantly dependent on the structure period, displaying much narrower FWHMs due to effective SPP excitations. Additional comparisons of angularly resolved scattering between Na nanorod and Na nanohole configurations (see details in Fig. S3 in the Supplementary Material) reveal that, unlike Na nanohole metasurfaces, which facilitate in-plane scattering and SPP excitations, Na nanorods are relatively poor lateral scatterers, confirming that Na nanorod arrays are ideal structures for minimizing SPP excitations. (2) Beyond structural properties, the electron density of Na nanorod is significantly lower than that of conventional noble metals such as silver. Consequently, Na nanorod metasurfaces exhibit longer-wavelength LSPR responses compared with silver counterparts with

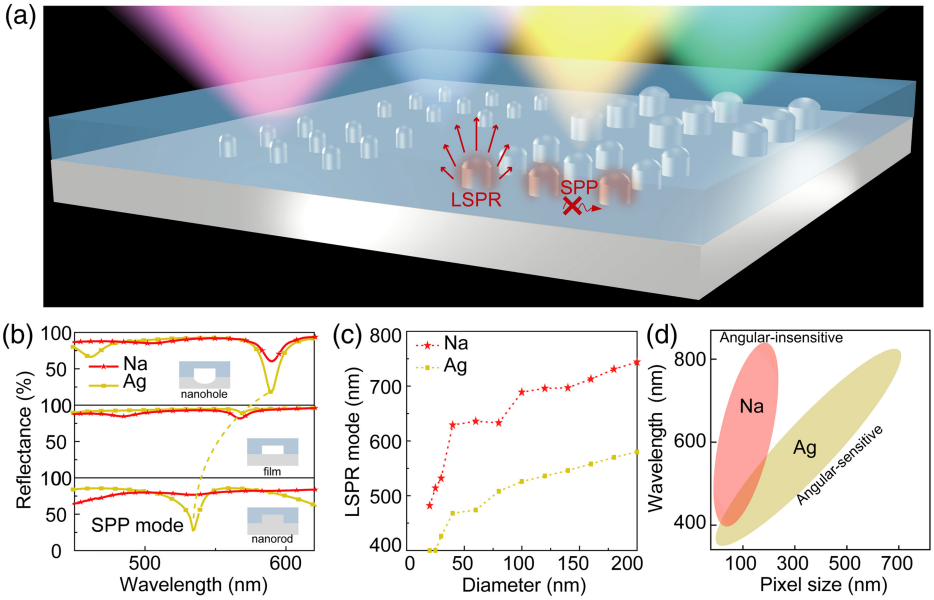

Fig. 1 Angular-robust plasmonic color devices based on sodium nanorod. (a) Schematic of Na plasmonic color devices with simple nanorod structures, featuring lateral period and angular-robust optical characterization. (b) Simulation reflectance spectra of three different structure configurations (nanohole, film, and nanorod) for Na ($p = 320$ nm, $d = 200$ nm, and $h = 50$ nm) and Ag ($p = 365$ nm, $d = 200$ nm, and $h = 50$ nm) showing different SPP mode strengths in the same resonance location. (c) Simulated single-particle plasmon mode (LSPR) location comparison of Na and Ag nanorods with a diameter (d) varying from 20 to 200 nm and a height (h) of 30 nm. (d) Comparison of Na and Ag nanorod-based plasmonic color devices.

identical geometric parameters (see details in Fig. 1(c) and Fig. S4 in the Supplementary Material). In addition, the Na nanorods provide better suppression of SPP effects than Ag nanorods, as depicted in Fig. 1(b). Therefore, the Na plasmonic structures offer optical advantages over traditional noble metals such as Ag, as shown in Fig. 1(d), allowing for flexible tuning of the color response through much smaller pixel sizes that are less sensitive to lateral period variations. This characteristic makes Na nanorods ideal for angle- and polarization-robust coloration, effectively mimicking pigment-based coloration under natural light illumination.

To experimentally achieve nanorod plasmonic coloration, we propose a rationally designed TSLM, effectively leveraging the unique optical and chemical properties of sodium, as schematically illustrated in Fig. 2(a). A quartz template with precisely defined geometrical parameters and wettability is used as the substrate, fabricated through FIB milling for proof-of-concept demonstration (refer to Sec. 2 and Figs. S5 and S6 in the Supplementary Material for further details). The TSLM procedure is then conducted to generate the nanorod metasurface based on the nanohole-patterned quartz substrate, utilizing sodium's low melting point (97.7°C) within an inert-atmosphere glove box (see Supplementary Material for additional details). By employing a lower liquid metal temperature and varying the droplet's location, we achieve a nanorod configuration distinct from the previously reported nanohole configurations.[38] The cross-sectional SEM image of the nanorod structure, displayed in Fig. 2(a), iii, clearly illustrates this configuration, which facilitates the suppression of SPP modes while enhancing LSPR dominance, resulting in angularly robust plasmonic colors. The templated quartz not only acts as an encapsulation layer but also improves light collection, ensuring long-term stability and enhancing viewing angle tolerance—key factors for practical color information applications.

To experimentally demonstrate the suppressed SPP and dominated LSPR of Na nanorods configuration, a series of Na nanorods plasmonic color palettes with different geometry parameters have been carefully designed and prepared. By flexibly tuning the period (p varies from 250 to 350 nm) of Na nanorod arrays with the same nanorod size ($d = 180$ nm and $h = 20$ nm) shown in Fig. 2(b), the optical modes of Na nanorod metasurfaces exhibit the period-immune spectroscopic feature. One may find that all the measured reflectance spectra of different periods exhibit the same reflection dip with broad linewidth (~100 nm) with no obvious SPP-based reflective dip (which is expected to be period dependent), and the corresponding optical micrographs show almost the same purple color with little difference, indicating the SPP mode suppression. However, the reflection dip and color are strongly dependent on the single pixel size of the Na nanorod metasurfaces [Fig. 2(c)] because of the dominant LSPR mode excitations. Thus, the structure color ranging from magenta, blue, cyan, and yellow can be well covered just by utilizing the simple Na nanorod metasurfaces without complicated manufacturing processes, evidencing that Na nanorods plasmonic color exhibits an appealing color library, as shown in Fig. S7 in the Supplementary Material. Notably, the durability test shows that the Na nanorod plasmonic colors exhibit no distinct color deterioration as exposed to ambient conditions for more than 40 days and can be further optimized by improving the sealing process, which is vital for practical applications (see Fig. S8 in the Supplementary Material).

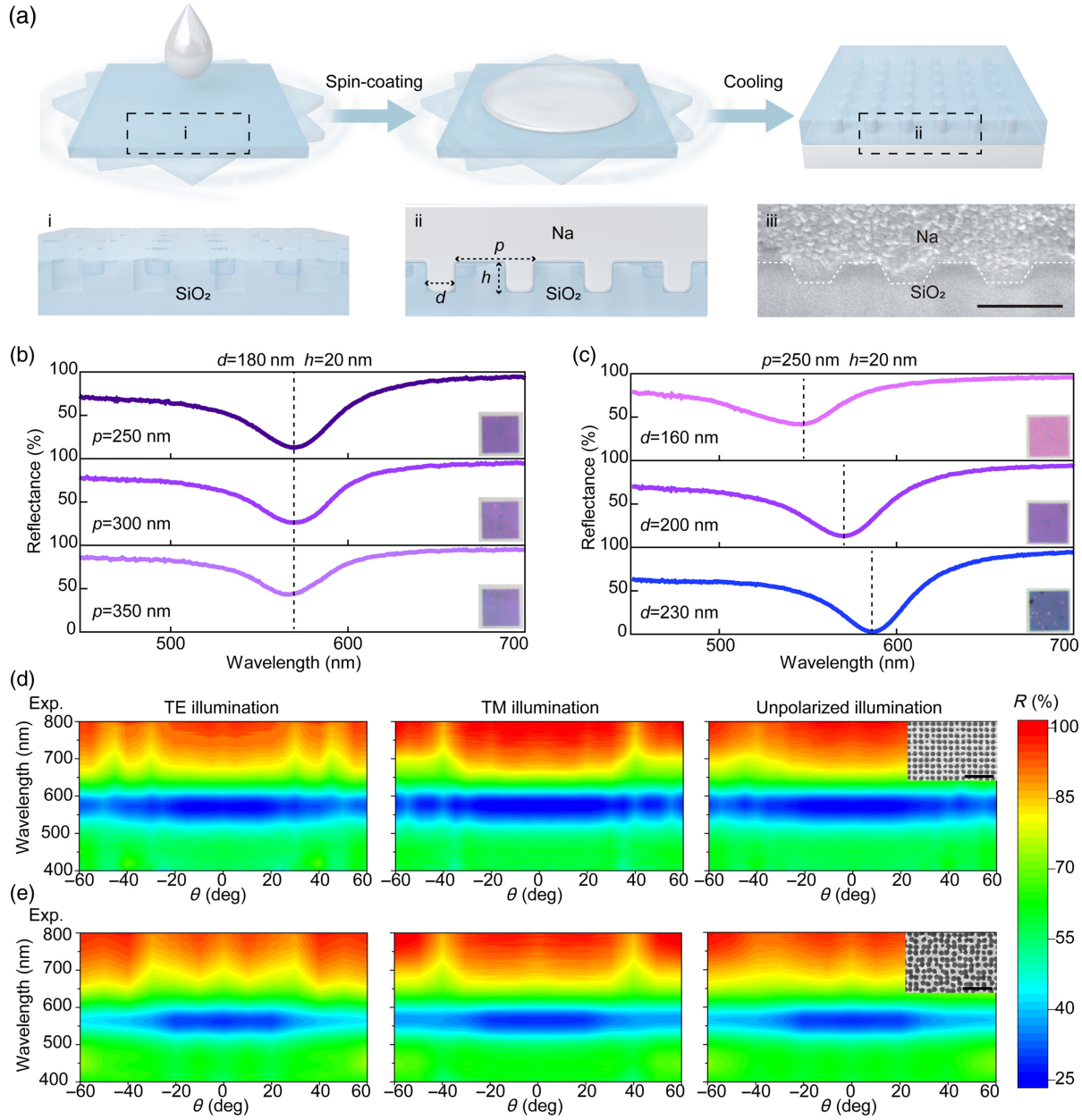

Fig. 2 Fabrication process and characterization of Na nanorods with varying structures. (a) Schematic of the thermo-assisted spin-coating method of fabrication of Na nanorods and the cross-sectional SEM images of Na nanorods (iii). The scale bar is 300 nm. (b) Experimental reflectance spectra of nanorod arrays with the same nanorod size and height (diameter $d = 180$ nm and height $h = 20$ nm) but different periods (p varies from 250 to 350 nm) under unpolarized incident light at 0 deg. (c) Experimental reflectance spectra of nanorod arrays with the same period and height ($p = 250$ nm and $h = 20$ nm) but different nanorod sizes (d varies from 160 to 230 nm) under unpolarized incident light at 0 deg. The insets are the corresponding optical images of nanorod arrays. (d) Experimental angular spectra of periodic Na nanorods of $p = 210$ nm, $d = 160$ nm, and $h = 30$ nm for TE polarization, TM polarization, and no polarization, and the inset is the SEM image of the corresponding device substrate. (e) Experimental angular spectra of random nanorods of $d = 160$ nm and $h = 30$ nm for TE polarization, TM polarization, and no polarization, and the inset is the SEM image of the corresponding device substrate. The scale bar is 1 μm.

Benefiting from the SPP suppression effect and strong LSPR mode extinction of Na nanorods configuration demonstrated above, one of the most intriguing properties of the proposed Na nanorod metasurfaces is the angular and polarization tolerance by fine-tuning the interplay of the LSP and SPP excitations, which is a crucial factor for well-defined structural colors in real-world scenarios. Figure 2(d) shows the up to 60-deg angle tolerance (limited by the numerical aperture of the objective lens in the measuring setup, see Sec. 2 for more details) and polarization tolerance of a representative Na nanorod metasurface ($p = 210$ nm, $d = 160$ nm, and $h = 30$ nm) measured by the angular resolved reflectance spectroscopy with transverse electric (TE), transverse magnetic (TM), and unpolarized illumination, respectively (see Sec. 2 for details). The experimental spectra agree well with the simulation results (Fig. S9 in the Supplementary Material) except for some slight deviations due to fabrication imperfection and variation of the nanostructures. The distinct single Lorentz profile optical mode in the entire visible spectrum evidences that the influence of the suppressed SPP mode is negligible, whereas the strong LSPR plays a major role in the color generation and is an intriguing candidate, with both priorities of structure colors (small pixel size and sustainability) and pigments (high angular tolerance). To further investigate the influence of periodicity, randomly positioned Na nanorods were fabricated (inset, SEM images) and examined. These nanorods exhibit similar angular and polarization tolerance without SPP excitation, indicating that the LSPR remains the dominant factor in optical performance, even without a defined periodic structure. This finding suggests that periodicity is not essential to maintain LSPR-based effects. However, periodic structures offer practical advantages for controlling optical responses. By setting unit cell positions based on a single parameter—the period—periodic designs can be optimized to enhance single-particle effects while reducing unwanted coupling. In contrast, random structures require complex positioning, as randomness negatively affects optical response through coupling effects and cell density (Fig. S10 in the Supplementary Material). Furthermore, periodic structures are amenable to scalable fabrication methods such as interference lithography, whereas intricate random structures present challenges in mass production. Experimental results further reveal that random Na nanorods exhibit reduced optical contrast compared with periodic arrangements (Fig. S11 in the Supplementary Material). Finally, deeper insights into the mechanisms can be obtained by comparing the simulated reflection spectrum of the periodic nanorods with the extinction cross section of single nanorod and single nanorod in periodic arrays of the same geometric size. The absorption dip position of the reflection spectrum of periodic nanorods is consistent with the position of the maximum extinction cross section of a single nanorod in or not in periodic arrays, respectively, further illustrating the primary role of the strong LSPR effect (Fig. S12 in the Supplementary Material).

To showcase the superior angle tolerance and pigment-like performance of the proposed Na nanorod metasurface, we compare its color gamut with Na film and Na nanohole configurations in Fig. S14 in the Supplementary Material. The angle-resolved color gamuts show consistent color coordinates for the Na nanorod configuration across incident angles (0 to 60 deg), highlighting the suppressed SPP and strong LSPR. In contrast, Na film and Na nanohole configurations exhibit angle-dependent spectra/color variations. In addition, the Na nanorod configuration boosts a larger color space due to its dominant LSPR mode, facilitating the creation of smaller, more saturated pigment-like nanopixels with reduced interparticle coupling.

In addition to the nanorod configuration advantages, it is noteworthy that the optical performances of the Na nanorod array surpass those of the Ag nanorod array in angular robustness and subwavelength spatial resolution. The angular resolved reflective spectra of the Na nanorod array are of higher angular tolerance than those for the Ag nanorod array (as depicted in Fig. 3). This improvement can be attributed to the more effective suppression of SPPs and higher field confinement in the Na nanorods compared with the Ag counterparts. In addition, the response wavelength of Na nanorods is much longer than that of corresponding Ag nanorods as demonstrated in Fig. 1(c), which is beneficial for achieving colorful pixels in smaller pixel sizes. It is obvious that the Ag nanorod arrays seem colorless, whereas the Na nanorod arrays are colorful in the same nanostructures shown in the insets of Figs. 3(d)–3(i). Figure S15 in the Supplementary Material illustrates a comparison of smaller configurations of Na and Ag nanorods. Consequently, leveraging both the Na material and the nanorod configuration advantages, Na nanorods display superior advantages in achieving colorful nanopixels with smaller pixel sizes and angular robustness akin to pigment-like hues.

Finally, as one of the most highly field-confined plasmonic metals, it is necessary to demonstrate the deep subwavelength spatial resolution of sodium-based photoprinting down to the single-pixel level. In the experiment, we have fabricated a series of samples consisting of 50×50, 20×20, 10×10, 4×4, and 2×2 sodium nanorods per pixel for different geometric parameters. Figure 4(a) exhibits the bright-field structural color for different-sized pixels of three primary colors: magenta, blue, and yellow from left to right, for which the parameters are $p = 260$ nm, $d = 150$ nm, and $h = 40$ nm; $p = 280$ nm, $d = 200$ nm, and $h = 60$ nm; and $p = 210$ nm, $d = 120$ nm, and $h = 30$ nm, respectively. Furthermore, the higher resolution optical performance of a single Na nanorod (d varying from 20 to 500 n and $h = 50$ nm) is measured in Fig. 4(b), demonstrating the subwavelength pixel size can be as small as 60 nm with well-preserved colors (also shown in Fig. S17 in the Supplementary Material). The dark-field optical image further demonstrates that the nanopixels can be clearly observed even with a single nanorod down to 40 nm (Fig. S18 in the Supplementary Material). Thus, the ultrahigh-resolution coloration performance of sodium metasurface with simple structure design and good angle-robustness is extremely attractive. Moreover, the angle tolerance can theoretically further reach 90 deg if randomly positioned sodium nanostructures are employed to suppress the directionality of LSPR far-field emission and eliminate the SPP effect.[41] Substrates with a higher refractive index can also be favorable for enabling up to 90-deg view-angle tolerance (Fig. S19 in the Supplementary Material). Therefore, this work can physically enable the intriguing angular robust color performance of up to 90 deg, an extremely high resolution of up to 60 nm per pixel, a simplified (and easily fabricated) structural design, and considerable optical contrast of 80% to 90% for optimized high-density nanostructures. These advantages make it superior to various structural coloration methods, as illustrated in Fig. 4(c), with detailed comparisons provided in Table S1 in the Supplementary Material.

Based on the attractively high-resolution feature and good coloration performance illustrated above, we further demonstrate

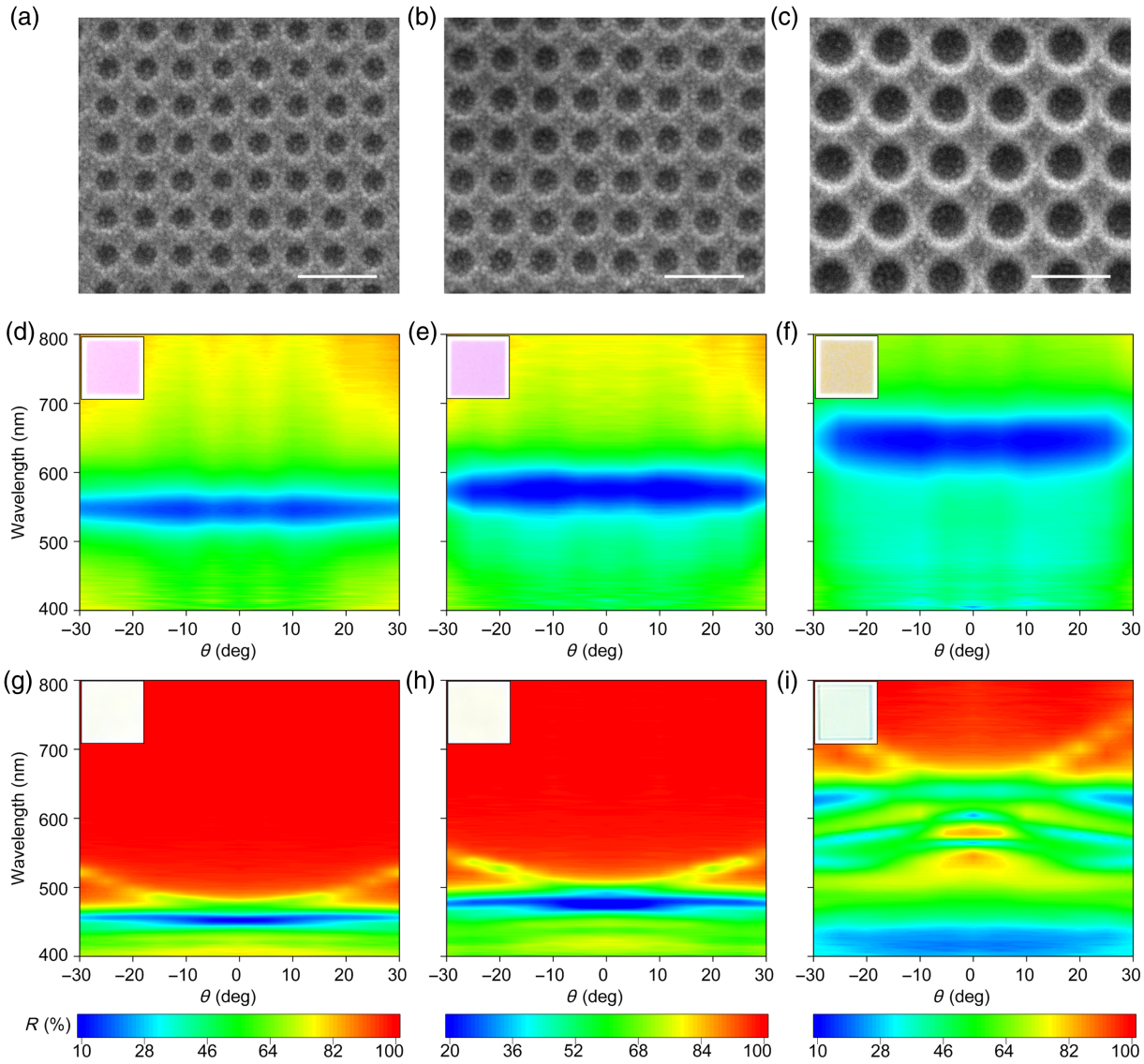

Fig. 3 Angular-insensitive optical characterization comparison of Na nanorod array and Ag nanorod array plasmonic color devices. SEM images of the quartz substrates with nanoholes of (a) $p = 240$ nm, $d = 120$ nm, and $h = 40$ nm; (b) $p = 260$ nm, $d = 150$ nm, and $h = 40$ nm; and (c) $p = 370$ nm, $d = 260$ nm, and $h = 70$ nm. The scale bar is 500 nm. (d)–(f) Experimental angular spectra of Na nanorods with nanostructures in panels (a)–(c) for unpolarized illumination, and the insets are microscope images of the corresponding Na nanorod patterns. (g)–(i) Experimental angular spectra of Ag nanorods with nanostructures in panels (a)–(c) for unpolarized illumination, and the insets are microscope images of the corresponding Ag nanorod patterns.

that our TSLM procedure is favorable for plasmonic nanopainting. The SEM images of different quartz substrates for plasmonic paintings of a colorful cartoon whale, colorful strips, colorful school badges, and the words "NANJING UNIVERSITY" are displayed in Fig. 4(d), and the bright-field optical micrographs of these plasmonic paintings at Kohler illumination are exhibited in Fig. 4(e). In real-world application scenarios, the angle-robust color nature is impressively illustrated. Here, the color information of "NANJING UNIVERSITY" lettering paintings is very consistent with a large viewing angle from 0 to 60 deg. Such an impressive view-angle tolerance can be ascribed to the LSPR-dominated response of the Na nanorod metasurface combined with the glass substrate-induced angle renormalization effect. The polarization independence of the plasmonic paintings is demonstrated in Fig. S20 in the Supplementary Material.

4 Conclusions

In summary, we have proposed and experimentally demonstrated ultrahigh-resolution plasmonic color devices with angle and polarization independence based on simple Na nanorod structures. This is achieved through the strong electromagnetic field confinement of sodium and minimal SPP excitation in the Na nanorod configuration, highlighting sodium as a promising

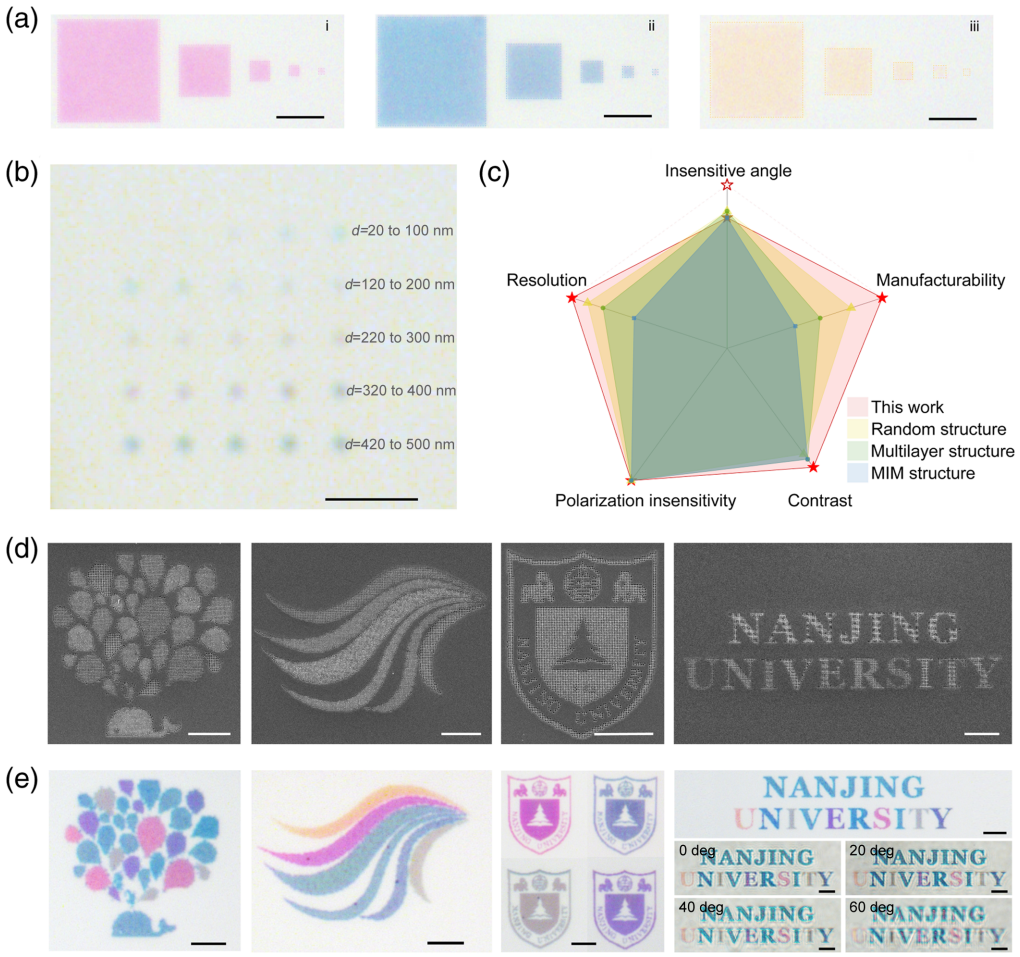

Fig. 4 Resolution test patterns and full-color image printing. (a) Bright-field optical micrographs of fabricated plasmonic color generation arrays with (i) $p = 260$ nm, $d = 150$ nm, and $h = 40$ nm; (ii) $p = 280$ nm, $d = 200$ nm, and $h = 60$ nm; and (iii) $p = 210$ nm, $d = 120$ nm, and $h = 30$ nm. (b) Bright-field optical micrograph of a single Na nanorod with d varying from 20 to 500 nm and $h = 50$ nm. (c) Comparison of different optical display research works in angle insensitivity, spatial resolution, manufacturability, polarization insensitivity, and contrast. (d) SEM images of the quartz substrates of colorful paintings of a cartoon whale, colorful strips, a school badge, and the words "NANJING UNIVERSITY." (e) Bright-field optical micrographs of a colorful cartoon whale, colorful strips, a school badge, the words "NANJING UNIVERSITY" taken at Kohler illumination, and micrographs of the words "NANJING UNIVERSITY" taken at fixed angle illumination of 0, 20, 40, and 60 deg. The scale bars are 5 μm in panels (a) and (b) and 10 μm in panels (d) and (e), respectively.

material for plasmonic color printing. In addition, Na nanorods naturally form a smooth nanostructured surface through liquid metal solidification, enabled by a straightforward thermo-assisted spin-coating process that avoids high-vacuum conditions. Both experimental results and simulations confirm that spectral properties can be finely tuned by adjusting the geometric parameters of Na nanostructures, achieving much smaller pixel sizes compared with traditional noble metals such as Ag. These Na nanostructures produce vibrant, angle-independent colors across the visible spectrum and maintain color stability at viewing angles exceeding ~60 deg. The combined advantages of high angular tolerance, ultrafine pixelation, and a cost-effective, scalable fabrication approach (e.g., UV lithography for substrate preparation) make this technique a strong candidate for high-throughput applications, including photoprinting and information storage.

Disclosures

The authors declare no conflicts of interest.

Code and Data Availability

The data that support the findings of this study are available from the corresponding authors upon reasonable request.

Acknowledgments

We acknowledge the microfabrication center of the National Laboratory of Solid State Microstructures for technical support. This work was supported by the National Key Research and Development Program of China (Grant Nos. 2021YFA1400700 and 2022YFA1404300), the National Natural Science Foundation of China (Grant Nos. 12022403 and 62375123),

and the Natural Science Foundation of Jiangsu Province (Grant No. BK20243009).

References

1. Y. Zhao et al., "Artificial structural color pixels: a review," *Materials* **10**, 944 (2017).
2. A. Kristensen et al., "Plasmonic colour generation," *Nat. Rev. Mater.* **2**, 16088 (2016).
3. M. Keshavarz Hedayati and M. Elbahri, "Review of metasurface plasmonic structural color," *Plasmonics* **12**, 1463–1479 (2016).
4. T. Lee et al., "Plasmonic- and dielectric-based structural coloring: from fundamentals to practical applications," *Nano Converg.* **5**, 1 (2018).
5. L. Shang et al., "Bio-inspired intelligent structural color materials," *Mater. Horiz.* **6**, 945–958 (2019).
6. I. Kim et al., "Pixelated bifunctional metasurface-driven dynamic vectorial holographic color prints for photonic security platform," *Nat. Commun.* **12**, 3614 (2021).
7. W. Yang et al., "All-dielectric metasurface for high-performance structural color," *Nat. Commun.* **11**, 1864 (2020).
8. Y. Wu et al., "TiO_2 metasurfaces: from visible planar photonics to photochemistry," *Sci. Adv.* **5**, eaax0939 (2019).
9. P. Cencillo-Abad et al., "Ultralight plasmonic structural color paint," *Sci. Adv.* **9**, eadf7207 (2023).
10. K. Li et al., "Facile full-color printing with a single transparent ink," *Sci. Adv.* **7**, eabh1992 (2021).
11. X. Zhu et al., "Resonant laser printing of structural colors on high-index dielectric metasurfaces," *Sci. Adv.* **3**, e1602487 (2017).
12. S. Jahani and Z. Jacob, "All-dielectric metamaterials," *Nat. Nanotechnol.* **11**, 23–36 (2016).
13. J. Kim et al., "A water-soluble label for food products prevents packaging waste and counterfeiting," *Nat. Food* **5**, 293–300 (2024).
14. S. A. Maier, Plasmonics: Fundamentals and Applications, Springer (2007).
15. J. Luo et al., "Plasmon-induced hot carrier dynamics and utilization," *Photonics Insights* **2**, R08 (2023).
16. M. Qiu et al., "Angular dispersions in terahertz metasurfaces: physics and applications," *Phys. Rev. Appl.* **9**, 054050 (2018).
17. X. Zhang et al., "Controlling angular dispersions in optical metasurfaces," *Light Sci. Appl.* **9**, 76 (2020).
18. V. G. Kravets et al., "Plasmonic surface lattice resonances: a review of properties and application," *Chem. Rev.* **118**, 5912–5951 (2018).
19. Y. Gu et al., "Color generation via subwavelength plasmonic nanostructures," *Nanoscale* **7**, 6409–6419 (2015).
20. K. T. Lee, S. Seo, and L. J. Guo, "High-color-purity subtractive color filters with a wide viewing angle based on plasmonic perfect absorbers," *Adv. Opt. Mater.* **3**, 347–352 (2015).
21. C. S. Park et al., "Omnidirectional color filters capitalizing on a nano-resonator of Ag-TiO_2-Ag integrated with a phase compensating dielectric overlay," *Sci. Rep.* **5**, 8467 (2015).
22. C. Song et al., "Angle-insensitive color filters based on multilayer ultrathin-film structures," *Plasmonics* **15**, 255–261 (2019).
23. C. Yang et al., "Compact multilayer film structure for angle insensitive color filtering," *Sci. Rep.* **5**, 9285 (2015).
24. B. M. Wells et al., "Angle-insensitive plasmonic nanorod metamaterial-based band-pass optical filters," *Opt. Express* **29**, 11562–11569 (2021).
25. A. M. Alam et al., "Generating color from polydisperse, near micron-sized TiO_2 particles," *ACS Appl. Mater. Interf.* **9**, 23941–23948 (2017).
26. D. Franklin et al., "Atomic layer deposition tuning of subwavelength aluminum grating for angle-insensitive plasmonic color," *ACS Appl. Nano Mater.* **1**, 5210–5216 (2018).
27. D. Franklin et al., "Self-assembled plasmonics for angle-independent structural color displays with actively addressed black states," *Proc. Natl. Acad. Sci. U. S. A.* **117**, 13350–13358 (2020).
28. Y. K. Wu et al., "Angle-insensitive structural colours based on metallic nanocavities and coloured pixels beyond the diffraction limit," *Sci. Rep.* **3**, 1194 (2013).
29. Q. J. Wu et al., "Plasmonic reflection color filters with metallic random nanostructures," *Nanotechnology* **28**, 085203 (2017).
30. J. Xue et al., "Semi-ellipsoid nanoarray for angle-independent plasmonic color printing," *Chin. Phys. Lett.* **37**, 114201 (2020).
31. A. Boltasseva and H. A. Atwater, "Low-loss plasmonic metamaterials," *Science* **331**, 290–291 (2011).
32. P. R. West et al., "Searching for better plasmonic materials," *Laser Photonics Rev.* **4**, 795–808 (2010).
33. Y. Wang et al., "Stable, high-performance sodium-based plasmonic devices in the near infrared," *Nature* **581**, 401–405 (2020).
34. J. Liang et al., "Lithium-plasmon-based low-powered dynamic color display," *Natl. Sci. Rev.* **10**, nwac120 (2023).
35. M. G. Blaber et al., "Plasmon absorption in nanospheres: a comparison of sodium, potassium, aluminium, silver and gold," *Phys. B Condens. Matter* **394**, 184–187 (2007).
36. Y. Jin et al., "In operando plasmonic monitoring of electrochemical evolution of lithium metal," *Proc. Natl. Acad. Sci. U. S. A.* **115**, 11168–11173 (2018).
37. A. Rawashdeh et al., "High-quality surface plasmon polaritons in large-area sodium nanostructures," *Nano Lett.* **23**, 469–475 (2023).
38. Y. Yang et al., "Sodium-based concave metasurfaces for high performing plasmonic optical filters by templated spin-on-sodiophobic-glass," *Adv. Mater.* **35**, e2300272 (2023).
39. Z. Gao et al., "Low-loss plasmonics with nanostructured potassium and sodium-potassium liquid alloys," *Nano Lett.* **23**, 7150–7156 (2023).
40. Y. Zhao et al., "Thermosensitive plasmonic color enabled by sodium metasurface," *Adv. Funct. Mater.* **33**, 2214492 (2023).
41. M. Ye et al., "Angle-insensitive plasmonic color filters with randomly distributed silver nanodisks," *Opt. Lett.* **40**, 4979–4982 (2015).

Jie Liang is a PhD student at the College of Engineering and Applied Sciences, Nanjing University. She is mainly engaged in research on alkali metal plasmonics and dynamic plasmonics based on electrochemistry.

Yurui Qu is a tenure-track assistant professor at the School of Information Science and Technology, ShanghaiTech University. He received his BS degree in optical engineering in 2014 and his PhD in 2019 at the Zhejiang University. Since 2019, he has been a postdoctoral research fellow and a research scientist at the University of Wisconsin-Madison. His research focuses on metamaterials, plasmonic devices, and optical artificial intelligence computing. His research has been recognized with over 2000 citations. He worked on alkali metal plasmonics in Nanjing University during 2022 to 2023.

Huizhen Zhang is a graduated master's student at the College of Engineering and Applied Sciences, Nanjing University.

Yuhan Yang is a PhD student at the College of Engineering and Applied Sciences, Nanjing University, with research interests in alkali metal plasmonics.

Yang Wang was a PhD student in Nanjing University and currently is an associated professor in Beijing Institute of Technology.

Yuchen Zhang is a PhD student at the College of Engineering and Applied Sciences, Nanjing University.

Zhenda Lu is a professor at the College of Engineering and Applied Sciences, Nanjing University.

Shining Zhu is a professor at the College of Engineering and Applied Sciences, Nanjing University, and an Academician of the Chinese Academy of Sciences.

Lin Zhou is a professor at the College of Engineering and Applied Sciences, Nanjing University. Her scientific research interest is in alkali metal plasmonics, nanophotonics, and light–matter coupling. Her research has been cited over 10000 times with an H-index of 39 in Google Scholar. She has been selected for the National Science Fund for Excellent Young Scholars and has been continuously listed as a Highly Cited Chinese Researcher and among the top 2% of the world's most-cited scientists.